M. J. D. Hayes
Mem. ASME
Assistant Professor,
Carleton University, Department of Mechanical & Aerospace Engineering,
Ottawa, Ontario, K1S 5B6, Canada

P. J. Zsombor-Murray
Mem. ASME
Associate Professor
McGill University, Dep't. of Mech. Eng. & Center for Intelligent Machines,
Montréal, Québec, H3A 2A7, Canada

C. Chen
Student Mem. ASME
Graduate Student,
McGill University, Dep't. of Mech. Eng. & Center for Intelligent Machines,
Montréal, Québec, H3A 2A7, Canada

Unified Kinematic Analysis of General Planar Parallel Manipulators

A kinematic mapping of planar displacements is used to derive generalized constraint equations having the form of ruled quadric surfaces in the image space. The forward kinematic problem for all three-legged, three-degree-of-freedom planar parallel manipulators thus reduces to determining the points of intersection of three of these constraint surfaces, one corresponding to each leg. The inverse kinematic solutions, though trivial, are implicit in the formulation of the constraint surface equations. Herein the forward kinematic solutions of planar parallel robots with arbitrary, mixed leg architecture are exposed completely, and in a unified way, for the first time. [DOI: 10.1115/1.1767186]

1 Introduction

A mapping of planar kinematics was introduced independently by Blaschke [1] and Grünwald [2] in 1911. Upon inspection, this planar kinematic mapping is a special case of Study's more general mapping of spatial kinematics [3]. In Study's mapping, rigid body displacements in three dimensional Euclidean space are transformed as points on a quadric surface, called *Study's quadric*, in a seven dimensional projective image space. The mapping is injective, hence only the points on Study's quadric have preimages in three-dimensional Euclidean space that are displacements. This means that for *every* Euclidean displacement there is a unique image point on Study's quadric.

Planar displacements are a subgroup of those in three-dimensional space. The planar kinematic mapping transforms displacements in the Euclidean plane into fundamental geometric elements (points) in a higher dimensional projective space. These points must also lie on Study's quadric, though on a bounded portion of it. Because the mapping is a linear transformation, the geometry that it implies allows for conceptual visualization of complicated kinematic problems in parallel mechanism analysis and synthesis. Such visualization leads to formulation of relatively simple surface intersection problems.

Transforming complicated algebraic problems into analogous, much simpler geometric ones is implicit in Klein's famous *Erlangen Program* [4]. Klein summarized this concept [5]: ''Given any group of linear transformations in space which includes the principal (Euclidean) group as a sub-group, then the invariant theory of this group gives a definite kind of geometry, and every possible geometry can be obtained in this way.'' Thus, the principles of planar Euclidean kinematics are completely described by the geometry of the image space.

The *forward kinematic* problem for in-parallel-actuated manipulators is a very complex problem: given the values of the inputs for the active joint in each leg, determine the position and orientation of the end-effector. The key to a generalized kinematic formulation, independent from specific leg architecture and actuation, is the characterization of platform displacements. Various Euclidean formulations were first used. Due to the nature of the forward kinematic problem, much of the earlier research concentrated on numerical solutions [6–9]. While numerical methods are essential for control, they yield no insight into theoretical issues, such as the size of the solution space, i.e., the number of possible assembly modes. Furthermore, many of these methods rely on an initial guess which must be fairly close to the solution in order to converge [8,10].

Many efforts have been made to provide some theoretical insight by viewing the problem from a different perspective. It was established by Hunt [11] that a planar three-legged platform with three RRR (or, when the middle joint is activated, the kinematically equivalent RPR)[1] legs admit at most six real assembly configurations for a given set of activated joint inputs. General solution procedures using elimination theory to derive a 6th degree univariate polynomial, which leads to all assembly configurations, were developed by Gosselin and Sefrioui [10] and Wohlhart [12], but only for platforms with three $R\underline{R}R$ or three $R\underline{P}R$ legs, with the underscore indicating the active joint. The forward kinematic problem is solved for a subset of the permutations of three-legged planar lower-pair-jointed three-legged platforms in Merlet [13]. However, because plane trigonometry is used to formulate the constraint equations, distinct architectures require distinct sets of equations, which are further dependent on platform geometry. The univariate polynomial for platforms consisting of three $R\underline{P}R$ legs was again derived by Pennock and Kassner [14], but the work was extended to include an investigation of the workspace [15]. Earlier work by Gosselin [16] provides a useful workspace optimization scheme for planar, spherical and spatial platform-type parallel manipulators. A detailed enumeration of assembly configurations of planar platforms can be found in Rooney and Earle [6]. Synthesis issues are addressed using a straightforward geometric approach by Shirkhodaie and Soni [9], while Murray and Pierrot [17] give an extremely elegant *n*-position synthesis algorithm, based on quaternions, for the design of planar platforms with three $R\underline{P}R$ legs.

What is lacking in the literature is a formulation of the kinematic geometry such that the metric trigonometric abstractions of a Euclidean geometric approach, leading to different representations of the constraints, can be unified in a single formulation that does not directly depend entirely on lengths, sines and cosines. Planar kinematic mapping leads to such a formulation that can be applied to the kinematic analysis, in particular to solve the forward and inverse kinematic[2] problems, of any lower pair jointed

Contributed by the Mechanisms and Robotics Committee for publication in the JOURNAL OF MECHANICAL DESIGN. Manuscript received July 2003; rev. Jan. 2004. Associate Editor: C. Mavroidis.

[1] R stands for *revolute* joint; P stands for *prismatic* joint.

[2] The inverse kinematic problem involves determining the required active joint values to attain a specified end-effector position and orientation.

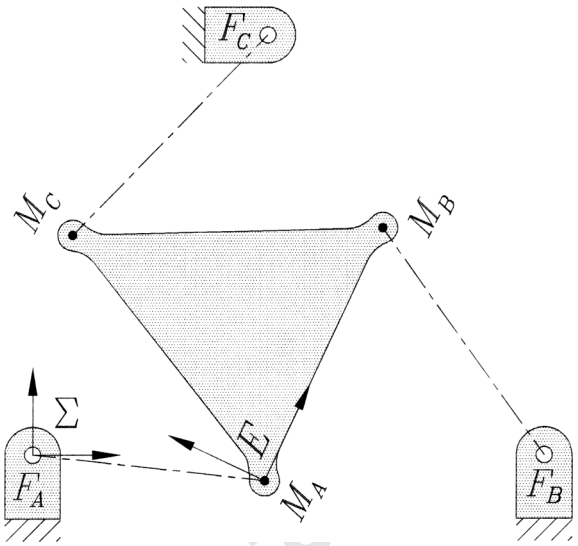

Fig. 1 The moving frame *E* and fixed frame Σ for any combination of legs from Table 1

three-legged platform with arbitrary leg architecture and actuation scheme. We provide the aforementioned formulation building on the work of Husty [18], Hayes [19], Chen [20], and Zsombor-Murray et al. [21].

In this paper, we present a single set of constraint equations that can be used to solve the inverse and forward kinematic problems of all possible lower pair jointed three legged planar platforms possessing three degrees of freedom (DOF), regardless of individual leg architecture and actuation. While the equations can be used for kinematic analysis of platforms with legs containing a serial chain combination of *R*- and/or *P*-pairs, it also applies to some architectures possessing holonomic, rolling higher pairs, *e.g.*, [22]. To start, we describe and enumerate the various designs using elementary counting principles. We continue with a brief review of planar kinematic mapping, then to derive and describe the image space constraint surfaces. Various applications to kinematic analysis are illustrated. In particular, application of these surfaces to the solution of forward kinematic problem is illustrated with three numerical examples. Finally, conclusions emphasize the results of this research and point out ways in which these might be fruitfully extended.

2 Classifying General Planar Three-Legged Platforms

A general planar three-legged platform with three DOF consists of a moving platform connected to a fixed base by three simple kinematic chains. Each chain is connected by three independent one DOF joints, one of which is active. Since the displacements of the platform are confined to the plane, only *R*- and *P*-pairs are used. But, in certain cases a holonomic higher gear pair (*G*) can replace a lower *R*-, or *P*-pair [22]. Platform motions are characterized by the motion of reference frame *E*, attached to the moving platform, relative to frame Σ, attached to the nonmoving base [23], see Fig. 1.

The possible combinations of *R*- and *P*-pairs which connect the moving platform to the fixed base and constrain the independent open kinematic chains, consisting of successions of three joints starting from the fixed base, in a three-legged platform are [13]:

$$RRR, RPR, RRP, RPP, PRR, PPR, PRP, PPP.$$

We must, however, exclude the PPP chain because no combination of pure planar translations can cause a change in orientation, such a leg would not possess three independent DOF. Thus, there are seven possible kinematic chains, which may be combined in either topologically symmetric or asymmetric groups of three.

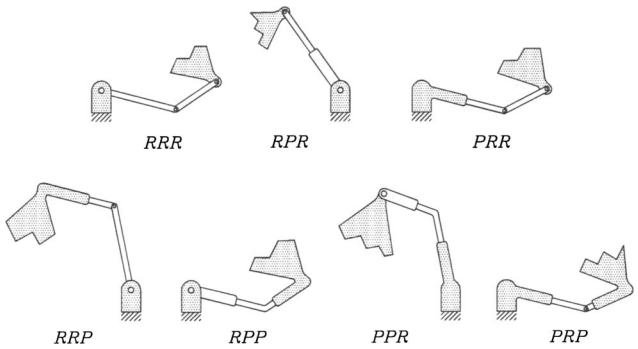

Fig. 2 The seven possible leg topologies

Figure 2 illustrates the seven possible simple kinematic chains. Proposed definitions of topological symmetry and asymmetry appear in the last paragraph in Section 2.1.

2.1 Passive Sub-Chains. The active joint in a leg is identified with an underscore, $R\underline{P}R$, for example. Since any one of the three joints in any of the seven allowable simple kinematic chains may be actuated there are twenty-one possible leg architectures. When the value of the actuated joint input in a leg is specified, the joint is effectively locked and may be conceptually removed, temporarily, from the chain. What remains is a kinematic chain connected with two passive joints. Examining Fig. 2, it is seen that the resulting passive sub-chain is one of only four types: either RR, PR, RP, or PP [13]. For the moment we exclude PP-type legs from the enumeration since platforms containing two or three such legs either move uncontrollably or are not assemblable when the actuated joint variables are specified [19]. Nonetheless, platforms containing one PP-type leg are feasible. They are considered separately. This reduces the number of possible leg architectures presently under consideration to eighteen. They are listed, according to passive sub-chain, in Table 1.

The platform is considered to be *symmetric* when all three legs are the same type, each possessing the same type of actuated joint at the same location in the kinematic chain. The platform is otherwise considered to be *asymmetric*.

2.2 Enumerating the General Planar Three-Legged Platforms. How many distinct general planar three-legged platforms with three DOF are there? This number is arrived at using elementary counting principles by first considering the 18 kinematic chains in Table 1 as the set to choose from for each leg. A selection of *r* different elements taken from a set of *n*, without regard to order, is a combination of the *n* elements taken *r* at a time. If the elements are allowed to be counted more than once the number of possible combinations is given by

$$C(n,r) = \frac{(n+r-1)!}{r!(n-1)!} \Rightarrow C(18,3) = 1140. \quad (1)$$

There are, in addition, three possible PP-type legs: $\underline{R}PP$, $P\underline{R}P$, and $PP\underline{R}$. However, a platform can only contain one

Table 1 18 of 21 possible lower pair leg architectures

RR-type	*PR*-type	*RP*-type
$\underline{R}RR$	$\underline{P}PR$	$\underline{R}RP$
$\bar{R}\underline{R}R$	$\bar{P}\underline{R}R$	$\bar{R}\underline{R}P$
$R\bar{R}\underline{R}$	$P\bar{R}\underline{R}$	$R\bar{P}\underline{R}$
$\underline{P}R\bar{R}$	$\underline{P}P\bar{R}$	$\underline{P}R\bar{P}$
$\bar{R}\underline{P}R$	$\bar{P}\underline{P}R$	$\bar{R}\underline{P}P$
$R\bar{R}\underline{P}$	$P\bar{R}\underline{P}$	$R\bar{P}\underline{P}$

PP-type leg. This one leg can be combined with any of the 18 listed in Table 1. The total number of platforms containing a single *PP*-type leg can therefore be counted as

$$3(C(18,2)) = 513. \tag{2}$$

Combining the results of Eqs. (1) and (2) gives the number of all possible general planar three-legged platforms, jointed with lower pairs, possessing three DOF: 1653. The kinematic analysis of all 1653 different platforms is accomplished using the single constraint formulation derived in what follows.

3 The Grünwald-Blaschke Mapping of Plane Kinematics

Consider the reference frame E which can undergo general planar displacements relative to reference frame Σ, as illustrated in Fig. 1. Let the homogeneous coordinates of points in the moving frame E be the ratios $(x:y:z)$, and homogeneous coordinates of the same point, but expressed in the fixed frame Σ, be the ratios $(X:Y:Z)$. The homogeneous transformation that maps the coordinates of points in E to Σ, which can also be viewed as a displacement of E relative to Σ, can be written as

$$\begin{bmatrix} X \\ Y \\ Z \end{bmatrix} = \begin{bmatrix} \cos\varphi & -\sin\varphi & a \\ \sin\varphi & \cos\varphi & b \\ 0 & 0 & 1 \end{bmatrix} \begin{bmatrix} x \\ y \\ z \end{bmatrix}. \tag{3}$$

Equation (3) indicates that a general planar displacement is characterized by the three parameters a, b, and φ, where a and b are the $(X/Z, Y/Z)$ coordinates of the origin of E expressed in Σ, and φ is the orientation of E relative to Σ, respectively.

Planar kinematic mapping [1,2] is described here briefly, but a very thorough discussion may be found in [23]. The essential idea is to map the three homogeneous coordinates of the pole of a planar displacement, in terms of (a,b,φ), to the points of a three-dimensional projective image space. Hence, the kinematic mapping image coordinates are defined as:

$$\begin{aligned} X_1 &= a\sin(\varphi/2) - b\cos(\varphi/2) \\ X_2 &= a\cos(\varphi/2) + b\sin(\varphi/2) \\ X_3 &= 2\sin(\varphi/2) \\ X_4 &= 2\cos(\varphi/2). \end{aligned} \tag{4}$$

Since each distinct displacement described by (a,b,φ) has a corresponding unique image point, the inverse mapping can be obtained from Eqs. (4): for a given point of the image space, the displacement parameters are

$$\begin{aligned} \tan(\varphi/2) &= X_3/X_4, \\ a &= 2(X_1X_3 + X_2X_4)/(X_3^2 + X_4^2), \\ b &= 2(X_2X_3 - X_1X_4)/(X_3^2 + X_4^2). \end{aligned} \tag{5}$$

Equations (5) give correct results when either X_3 or X_4 is zero. Caution is in order, however, because the mapping is injective, not bijective: *there is at most one pre-image for each image point*. Thus, not every point in the image space represents a displacement. It is easy to see that any image point on the real line $X_3 = X_4 = 0$ has no preimage and therefore does not correspond to a real displacement of E. From Eqs. (5), this condition renders φ indeterminate and places a and b on the line at infinity. We call this the *nonzero condition* and define it as $X_3^2 + X_4^2 \neq 0$. The existence of a pre-image depends on this condition being satisfied. It represents exactly the portion of Study's quadric corresponding to rigid body displacements in the Euclidean plane.

By virtue of the relationships expressed by Eqs. (4), the transformation matrix from Eq. (3) may be expressed in terms of the homogeneous coordinates of the image space. This yields a linear transformation to express a displacement of E with respect to Σ in terms of the image point [23]:

$$\lambda \begin{bmatrix} X \\ Y \\ Z \end{bmatrix} = T \begin{bmatrix} x \\ y \\ z \end{bmatrix}, \tag{6}$$

where λ is some nonzero constant arising from the use of homogeneous coordinates and

$$T = \begin{bmatrix} X_4^2 - X_3^2 & -2X_3X_4 & 2(X_1X_3 + X_2X_4) \\ 2X_3X_4 & X_4^2 - X_3^2 & 2(X_2X_3 - X_1X_4) \\ 0 & 0 & X_3^2 + X_4^2 \end{bmatrix}.$$

The inverse transformation can be obtained with the inverse of the matrix in Eq. (6) as follows.

$$\gamma \begin{bmatrix} x \\ y \\ z \end{bmatrix} = T^{-1} \begin{bmatrix} X \\ Y \\ Z \end{bmatrix}, \tag{7}$$

with γ being another nonzero constant arising from the use of homogeneous coordinates and

$$T^{-1} = \begin{bmatrix} X_4^2 - X_3^2 & 2X_3X_4 & 2(X_1X_3 - X_2X_4) \\ -2X_3X_4 & X_4^2 - X_3^2 & 2(X_2X_3 + X_1X_4) \\ 0 & 0 & X_3^2 + X_4^2 \end{bmatrix}.$$

Thus, the coordinates of a point $(x:y:z)$ in the (relatively) moving frame has coordinates $(X:Y:Z)$ in the (relatively) fixed frame:

$$\begin{aligned} X &= (X_4^2 - X_3^2)x - (2X_3X_4)y + 2(X_1X_3 + X_2X_4)z, \\ Y &= (2X_3X_4)x + (X_4^2 - X_3^2)y + 2(X_2X_3 - X_1X_4)z, \\ Z &= (X_3^2 + X_4^2)z. \end{aligned} \tag{8}$$

While the kinematic inversion requires the algebraic inverse, i.e. coordinates of a point $(X:Y:Z)$ in the (relatively) moving frame has coordinates $(x:y:z)$ in the (relatively) fixed frame which are given by:

$$\begin{aligned} x &= (X_4^2 - X_3^2)X + (2X_3X_4)Y + 2(X_1X_3 - X_2X_4)Z, \\ y &= -(2X_3X_4)X + (X_4^2 - X_3^2)Y + 2(X_2X_3 + X_1X_4)Z, \\ z &= (X_3^2 + X_4^2)Z. \end{aligned} \tag{9}$$

4 Kinematic Constraints

The aim of this section is to identify all possible kinematic constraints for general planar three-legged platforms corresponding to all the different leg architectures. There is a specific type of constrained motion corresponding to each of the passive subchains: *RR*-type; *PR*-type; *RP*-type; and *PP*-type. Because a motion is a continuous set of displacements, and because a displacement maps to a point, a constrained motion will map to a continuous set of points in the image space. As shown in [24], the constraints imposed by the four different leg types are quadric surfaces with special properties in the image space. To derive an expression for the kinematic constraint surface for a particular leg in the platform, we consider the individual leg, together with the moving platform, when the platform connections to the remaining legs have been severed. Now, consider the motion of a point with fixed coordinates in E, as E moves relative to Σ.

The lower-pair constraints on the motion of any particular leg in an arbitrary general planar three-legged platform involve only one of the following:

1. *RR*-type circular constraint: a point with fixed coordinates in the moving frame moves on a circle of fixed center and radius in the fixed frame.

2. *PR*-type linear constraint: a point with fixed point coordinates in the moving frame moves on a line with fixed line coordinates in the fixed frame.

3. *RP*-type linear constraint: a line with fixed line coordinates in the moving frame moves on a point with fixed point coordinates in the fixed frame.

4. *PP*-type planar constraint: a line with fixed line coordinates in the moving frame moves in the direction of a line with fixed line coordinates in the fixed frame (i.e., the distal *P*-pair moves in the direction of the ground-fixed *P*-pair).

It may be argued that the *RR*-type circular constraint is, in a sense, the most general, since a line can always be considered as a circle of infinite radius. The *PR*- and *RP*-type linear constraints are simply kinematic inversions. While the *PP*-type planar constraint is a special case.

4.1 Implicit Equation of the General Constraint Surface A clearer picture of the image space constraint surface that corresponds to the kinematic constraints described above emerges when $(X:Y:Z)$, or $(x:y:z)$ from Eqs. (8), or (9) are substituted into the general equation of a circle, the form of the most general constraint:

$$K_0(X^2+Y^2)+2K_1XZ+2K_2YZ+K_3Z^2=0, \tag{10}$$

where $[K_0:K_1:K_2:K_3]$ are the *circle coefficients*, with $K_1=-X_c$, $K_2=-Y_c$, $K_3=X_c^2+Y_c^2-r^2$, X_c and Y_c being the coordinates of the circle center of radius r, and K_0 is an arbitrary homogenising constant. One obtains the following quartic in X_i, which factors into two quadrics:

$$\begin{aligned}(K_0z^2(X_1^2+X_2^2)&+(-K_0x+K_1z)zX_1X_3+(-K_0y+K_2z)zX_2X_3\\ &\mp(K_0y+K_2z)zX_1X_4\pm(K_0x+K_1z)zX_2X_4\mp(K_1y-K_2x)\\ &\times zX_3X_4+\tfrac{1}{4}[K_0(x^2+y^2)-2z(K_1x+K_2y)+K_3z^2]X_3^2\\ &+\tfrac{1}{4}[K_0(x^2+y^2)+2z(K_1x+K_2y)+K_3z^2]X_4^2)\\ &\times(\tfrac{1}{4}(X_3^2+X_4^2))=0.\end{aligned} \tag{11}$$

The factor $1/4(X_3^2+X_4^2)$ is exactly the nonzero condition of the planar kinematic mapping, the planar analog to Study's quadric, which must be satisfied for a point to be the image of a real displacement. Since only the images of real displacements are considered, this factor must be nonzero and may be safely eliminated. In other words, images of real displacements have image space coordinates such that X_3 and X_4 are not both zero, so we may safely divide this first factor out of Eq. (11). What remains is a quadratic in the X_i. The quantities x, y, z (coordinates of leg-platform attachment points which have fixed position in E) and K_i are all design constants. Hence, the first factor in Eq. (11) is the point equation of a quadric surface in the three-dimensional projective image space. This quadric is the geometric image of the kinematic constraint that a point with fixed point coordinates in the moving reference frame moves on either a fixed circle, or a fixed line, in the fixed reference frame depending on whether $K_0=1$, or $K_0=0$, respectively. If the kinematic constraint is a point with fixed coordinates in E bound to a circle $(K_0=1)$, or line $(K_0=0)$ with fixed coordinates in Σ, then $(x:y:z)$ are the coordinates of the platform reference point in E and the upper signs apply. Alternately, if the kinematic constraint is a point with fixed coordinates in Σ bound to a circle $(K_0=1)$ with fixed circle coordinates, or line $(K_0=0)$ with fixed line coordinates in E, then $(X:Y:Z)$ are substituted for $(x:y:z)$, and the lower signs apply.

The first factor in Eq. (11) is greatly simplified under the following assumptions:

1. No platform of practical significance will have a point at infinity, so it is safe to set $z=1$.

2. Platform rotations of $\varphi=\pi$ (half-turns) have images in the plane $X_4=0$. Because the X_i are implicitly defined by Eq. (4), setting $\varphi=\pi$ gives

$$(X_1:X_2:X_3:X_4)=(a:b:2:0). \tag{12}$$

When we remove the one parameter family of image points for platform orientations of $\varphi=\pi$ we can, for convenience, normalize the image space coordinates by setting $X_4=1$. Conceptually, this implies dividing the X_i by $X_4=2\cos\varphi/2$ giving

$$\begin{aligned}X_1&=\tfrac{1}{2}(a\tan(\varphi/2)-b)\\ X_2&=\tfrac{1}{2}(a+b\tan(\varphi/2))\\ X_3&=\tan(\varphi/2)\\ X_4&=1.\end{aligned} \tag{13}$$

Applying these assumptions to the first factor in Eq. (11) gives the simplified constraint surface equation:

$$\begin{aligned}K_0(X_1^2+X_2^2)&+(-K_0x+K_1)X_1X_3+(-K_0y+K_2)X_2X_3\mp(K_0y\\ &+K_2)X_1\pm(K_0x+K_1)X_2\mp(K_1y-K_2x)X_3+\tfrac{1}{4}[K_0(x^2+y^2)\\ &-2(K_1x+K_2y)+K_3]X_3^2+\tfrac{1}{4}[K_0(x^2+y^2)+2(K_1x+K_2y)\\ &+K_3]=0.\end{aligned} \tag{14}$$

The K_i in Eq. (14) are functions of the variable joint input parameter. As shown in [24], the surface is an hyperboloid of one sheet when $K_0=1$, and is an hyperbolic paraboloid when $K_0=0$.

4.2 *RR*-Type Circular Constraints. The ungrounded *R*-pair in an *RR*-type leg is constrained to move on a circle with a fixed radius and center coordinates. Meanwhile, the platform can rotate about the moving *R*-pair when the platform connections of the other two legs have been opened. This two parameter family of displacements corresponds to a two parameter hyperboloid of one sheet in the image space. An important property of the hyperboloid is that sections in planes parallel to $X_3=0$ are circles [23,24]. One of these image space circles represents possible platform displacements with a fixed orientation. Thus the constraints imposed by *RR*-type legs are called *circular constraints*. The exact coefficients of the hyperboloid are determined by substituting in Eq. (14) the appropriate values for the kinematic parameters:

$$\begin{aligned}K_0&=1,\\ K_1&=-X_c,\\ K_2&=-Y_c,\\ K_3&=K_1^2+K_2^2-r^2,\end{aligned} \tag{15}$$

where (X_c,Y_c) are the coordinates of the fixed circle center in the fixed frame, and r is the circle radius. If the kinematic constraint is a fixed point in E bound to fixed circle in Σ, then (x,y) are the coordinates of the platform reference point in E, and the upper signs in Equation (14) apply. If the kinematic constraint is a fixed point in Σ bound to fixed circle in E, then the (X,Y) coordinates of the platform reference point in Σ are substituted for (x,y), and the lower signs in Eq. (14) apply.

4.3 *PR*- and *RP*-Type Linear Constraints. Using geometric arguments similar to those for the circular constraints, the kinematic constraints imposed by *PR*- and *RP*-type legs are called *linear constraints*. If $K_0=0$ then Eq. (10) becomes

$$Z(2K_1X+2K_2Y+K_3Z)=0. \tag{16}$$

Equation (16) represents two lines. The factor $Z=0$ is the line at infinity in the projective plane, P_2, while the factor in parentheses is the equation of a line where the first two *line coordinates* are multiplied by 2. The 2 can be treated as a proportionality factor arising from the original circle formulation of the equation of

constraint. The ratios $(X:Y:Z)$ are homogeneous coordinates the points on the line defined by K_1, K_2, and K_3. Dually, the K_1, K_2, and K_3 are the homogeneous coordinates of the lines on the point defined by $(X:Y:Z)$. The *trivial* factor $Z=0$ can be ignored because only ordinary lines (nonideal lines) need be considered for practical designs. Looking at Eq. (16) it is to be seen that

$$[K_1:K_2:K_3]=[\tfrac{1}{2}L_1:\tfrac{1}{2}L_2:L_3], \tag{17}$$

where the L_i are line coordinates obtained by Grassmann expansion of the determinant of two points on the line [5].

An $\underline{R}PR$ leg will be used for illustration. For these legs the line coordinates are determined by the base *R*-pair inputs and the corresponding center point of the ground fixed *R*-pair, F_i, $i \in \{A,B,C\}$ (see Fig. 1). The direction of the line is given by the base *R*-pair input: the joint angle with respect to the fixed base frame Σ, ϑ_Σ. The line equation in Σ for a given leg is obtained from the Grassmann expansion:

$$\begin{vmatrix} X & Y & Z \\ F_{X/\Sigma} & F_{Y/\Sigma} & F_{Z/\Sigma} \\ \cos\vartheta_\Sigma & \sin\vartheta_\Sigma & 0 \end{vmatrix} = 0, \tag{18}$$

where the notation $F_{X/\Sigma}$, $F_{Y/\Sigma}$, $F_{Z/\Sigma}$, represent the homogeneous coordinates, in reference frame Σ, of the revolute center that is fixed relative to Σ. Expanding this determinant yields the equation of the line:

$$-F_{Z/\Sigma}\sin\vartheta_\Sigma X + F_{Z/\Sigma}\cos\vartheta_\Sigma Y + (F_{X/\Sigma}\sin\vartheta_\Sigma - F_{Y/\Sigma}\cos\vartheta_\Sigma)Z = 0. \tag{19}$$

The L_i line coordinates are the respective coefficients of *X*, *Y*, and *Z*. Applying Eq. (17) we obtain

$$[K_1:K_2:K_3]=\left[-\frac{F_{Z/\Sigma}}{2}\sin\vartheta_\Sigma:\frac{F_{Z/\Sigma}}{2}\cos\vartheta_\Sigma:(F_{X/\Sigma}\sin\vartheta_\Sigma - F_{Y/\Sigma}\cos\vartheta_\Sigma)\right]. \tag{20}$$

For a particular input angle of the actuated joint, ϑ_Σ, we obtain the line coefficients $[K_1:K_2:K_3]$. These, after setting $K_0=0$, along with the design values of the coordinates of the platform reference point (x,y), expressed in reference frame *E*, are substituted into Eq. (14). Using the upper signs reveals the image space constraint surface for the given leg, input values, and kinematic constraints. This surface is an hyperbolic paraboloid with one regulus ruled by skew lines that are all parallel to the plane $X_3=0$ [24].

The kinematic inversion of the $\underline{R}PR$ leg is the $RP\underline{R}$. In this case the kinematic constraint can be described as a point with fixed coordinates in Σ constrained to move on a line with fixed line coordinates in *E*. We now replace (x,y) with (X,Y), the coordinates of the point expressed in Σ (after setting $z=Z=1$), and use the lower signs in Eq. (14). Furthermore, the line equation is defined as

$$\begin{vmatrix} x & y & z \\ M_{x/E} & M_{y/E} & M_{z/E} \\ \cos\vartheta_E & \sin\vartheta_E & 0 \end{vmatrix} = 0, \tag{21}$$

where the notation $M_{x/E}$, $M_{y/E}$, $M_{z/E}$, represent the homogeneous coordinates $(x:y:z)$, in reference frame *E*, of the revolute center that is fixed relative to *E*. Applying Eq. (17) we obtain

$$[K_1:K_2:K_3]=\left[-\frac{M_{z/E}}{2}\sin\vartheta_E:\frac{M_{z/E}}{2}\cos\vartheta_E:(M_{x/E}\sin\vartheta_E - M_{y/E}\cos\vartheta_E)\right]. \tag{22}$$

Similar simple arguments, based on the kinematic constraints for the leg, reveal the pertinent line coordinates as in Eqs. (20) and (22) for any *PR*- or *RP*-type leg, respectively.

4.4 *PP*-Type Planar Constraints. Recall that *PP*-type legs must contain an active *R*-pair. The kinematic constraints imposed by *PP*-type legs are called *planar constraints* for the following reason. The image space constraint surface corresponding to possible displacements of a *PP*-type leg is a degenerate quadric that splits into a real and an imaginary plane. This is because only curvilinear motion of the platform can result when the other two platform attachment joints are disconnected: once the angular input of the active *R*-pair is fixed no rotation of leg or platform is possible. The image of a two parameter family of displacements must be a two parameter constraint manifold, but because φ is constant, the image space coordinates $X_3=f(\varphi)$ and $X_4=g(\varphi)$ must also be constant. Hence, the finite part of the two-dimensional constraint manifold is linear and must be a hyper-plane.

All planes corresponding to possible displacements of the *PP*-type leg are parallel to $X_3=0$. if the platform consists of two or three *PP*-type legs, the constraint planes may be distinct but parallel, thereby having no finite points in common; or the planes will be coincident, indicating infinite assembly modes yielding uncontrollable self motions. There is no practical design merit associated with platforms containing two, or three *PP*-type legs. This, however, does not preclude designs of topologically asymmetrical three legged planar platforms with at most one *PP*-type leg. On the other hand, the self-motion property provides possibilities to design very stiff one DOF planar platforms which are relatively easy to actuate.

Regardless, in this paper we are only interested in general planar three-legged platforms possessing three DOF, thus only one of the three legs can be a *PP*-type for the platform to be assemblable and have three DOF. When the active *R* joint in the *PP*-type leg is locked, points on the distal *P*-pair are constrained to move on a plane. The kinematic mapping image of this constraint maps to the finite portion of the plane in the image space. The plane is completely determined by the platform orientation, which is implicitly determined by the active *R*-pair input to the *PP*-type leg. When the image space is normalized by setting $X_4=1$, the platform orientation is proportional to X_3:

$$X_3=\tan(\varphi/2). \tag{23}$$

5 The Inverse Kinematic Problem

The inverse kinematic problem may be stated as: given the position and orientation of the platform frame *E*, determine the variable joint inputs and corresponding assembly modes required for the moving platform to attain the desired pose. Establishing the inverse kinematics is essential for the position control of parallel manipulators. Fortunately, the inverse kinematics are trivial, and closed form algebraic solutions can usually be found.

To begin, one observes that the forward kinematic problem reduces to determining the intersection points of three constraint surfaces in the projective image space. Each point of intersection represents a platform pose. It follows that the inverse kinematic problem can be solved by working in the opposite direction: start with a given point in the image space which represents a feasible platform pose and extract a set of active joint inputs from the corresponding pre-image. Because the mapping is not bijective there is at most one pre-image for every point in the image space.

With the use of kinematic mapping it is a simple matter to determine all inverse kinematic solutions by considering the general constraint surface for each leg of the platform in question. Each leg of the platform can be considered separately because the solutions are decoupled from leg-to-leg [16]. Hence, the inverse kinematic problem of every lower pair jointed three-legged planar platform with three DOF can be solved by determining the joint input value from the image point satisfying the associated con-

straint surface equation. Moreover, the inverse kinematic problem for $RR\underline{C}$-type platforms are also easily determined, which is not possible with conventional Cartesian approaches due to the ambiguities introduced by the relative rolling between each gear pair [25,26].

5.1 Circular Constraints. For all RR-type legs the joint input in the ith leg can always be characterized as the distance between the fixed base point, F_i, and the moving platform point, M_i, regardless of the active joint type. This distance is the radius r of the constraint circle, all other quantities being constants. After substituting $K_3 = K_1^2 + K_2^2 - r^2$ into Eq. (14) then expanding and collecting in terms of r yields a quadratic having the form:

$$Ar^2 + Br + C = 0, \tag{24}$$

where

$$A = -z^2(X_3^4 + X_4^4),$$

$$B = 0,$$

$$C = 4z^2(X_1^2 + X_2^2) + (z^2(K_1^2 + K_2^2) - 2z(K_1x + K_2y) + x^2 + y^2)X_3^2 + (z^2(K_1^2 + K_2^2) + 2z(K_1x + K_2y) + x^2 + y^2)X_4^2 + 4z[(K_1z - x)X_1X_3 \mp (K_2 + y)X_1X_4 + (K_2z - y)X_2X_3 \pm (K_1z + x)X_2X_4 \pm (K_2x - K_1y)X_3X_4].$$

While this result means that there are two real solutions, only one is acceptable since the quantity represents the radius of a circle, which is, by convention, a positive nonzero number. Thus, there is but one solution for a given RR-type platform leg:

$$r = \left| \frac{\sqrt{-AC}}{A} \right|. \tag{25}$$

The fact that there is but one value for r does not, in general, mean that there is but one solution to the inverse kinematic problem. Only the $R\underline{P}R$-type leg has a unique solution, all other RR-types have *elbow-up* and *elbow-down* solutions.

5.2 Linear Constraints. Inverse kinematic solutions for PR- and RP-type sub-chains is accomplished by solving the general constraint equation for a single variable: the unknown direction of the line joining the F_i and the corresponding M_i. Here the planar line coordinates are defined as:

$$K_0 = 0,$$

$$K_1 = -\tfrac{1}{2} Z \sin \iota,$$

$$K_2 = \tfrac{1}{2} Z \cos \iota,$$

$$K_3 = R = X \sin \iota - Y \cos \iota,$$

where the $(X{:}Y{:}Z)$ are the homogeneous coordinates of the fixed base point, and the unknown is ι, the angle the line makes with the X-axis. Making the appropriate substitutions in Eq. (14) gives an equation linear in the sines and cosines of ι. Solving for ι gives:

$$\iota = \operatorname{atan} 2(N, D), \tag{26}$$

where

$$N = 2zZ(X_1X_4 - X_2X_3) - 2xZX_3X_4 + (yZ + zY)X_3^2 + (zY - yZ)X_4^2$$

$$D = -2zZ(X_1X_3 + X_2X_4) + 2yZX_3X_4 + (xZ + zX)X_3^2 + (zX - xZ)X_4^2$$

The input parameter for each PR- or RP-type leg required to attain the given pose is easily obtained from the calculated value of ι using plane trigonometry and known design parameters. As for the RR-type legs, there is but one solution for this equation per PR- or RP-type leg, but not in general to the inverse kinematic problem which can have as many as $2^3 = 8$ real solutions.

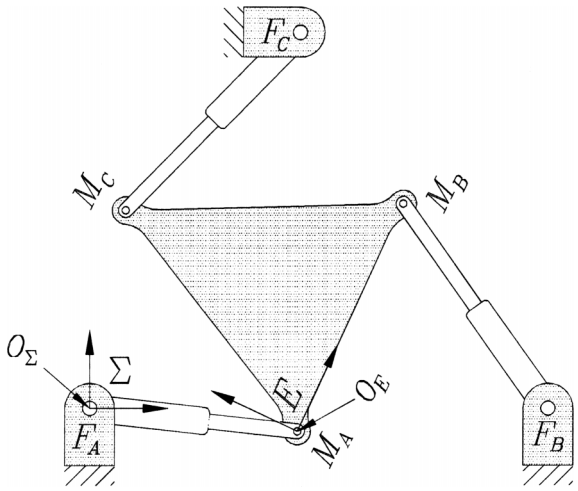

Fig. 3 A platform with three *RPR* legs

5.3 Planar Constraints. In the case of a PP-type leg the inverse kinematics depends entirely upon the orientation of the end-effector. The input R-pair value is then found simply by summing the appropriate angles.

6 The Forward Kinematic Problem: Examples

For in-parallel actuated manipulators the forward kinematic problem is not as elementary as the inverse kinematics. It consists of determining the pose of the moving platform, described by the position and orientation of reference frame E relative to reference frame Σ given the values for the inputs of the active joints in each of the three legs. The following three examples illustrate the applications of the constraint surface formulation to solve the forward kinematic problem.

6.1 Symmetric $R\underline{P}R$ Platform. The classic example of the forward kinematic problem for planar manipulators involves three architecturally symmetric RR-type legs [10,12,18]. These examples use either three identical $R\underline{P}R$, or kinematically equivalent $R\underline{R}R$ legs. The platform shown in Fig. 3 can be used to illustrate both symmetric and asymmetric platforms, depending on which joint in each leg is active.

To simplify the form of the constraint surfaces, it is convenient to assign reference frames E and Σ as in Fig. 3. To describe the platform, the three legs are identified as A, B, and C. The *fixed* reference points, where each leg is attached to a rigid, nonmoving frame, are F_i, $i \in \{A,B,C\}$. The *moving* reference points, where each leg is connected to the platform, are M_i, $i \in \{A,B,C\}$. The origin of Σ, O_Σ, is on F_A. Homogeneous coordinates in Σ are described by the triples of ratios $(X{:}Y{:}Z)$. The fixed reference point on leg B, F_B, is on the positive X-axis. The origin of E, O_E, is on M_A. Homogeneous coordinates in E are described by the triples of ratios $(x{:}y{:}z)$. The moving reference point in leg B, M_B, is on the positive x-axis. The classic forward kinematic problem requires placing the vertices of the moving triangle on the three circles defined by the fixed triangle and given leg lengths.

This example is taken from [18]. The base and platform geometry, and variable joint inputs are listed in Table 2. The homogeneous coordinates $(X{:}Y{:}Z)$ of the circle centers, expressed in Σ, are indicated by the $F_{i/\Sigma}$. The homogeneous coordinates $(x{:}y{:}z)$ of the platform reference points, expressed in E, bound to the respective circles are indicated by the $M_{i/E}$. The radii of the respective circles, determined by the lengths of the three active prismatic joints are given by r_i. The circle coefficients, K_i, are determined according to Eqs. (15).

Table 2 *RPR* geometry, joint inputs and circle coefficients

i	$F_{i/\Sigma}:(X:Y:Z)$	$M_{i/E}:(x:y:z)$	r_i	$(K_{0_i}:K_{1_i}:K_{2_i}:K_{3_i})$
A	(0:0:1)	(0:0:1)	1	(1:0:0:−1)
B	(3:0:1)	(2:0:1)	2	(1:−3:0:5)
C	(1:3:1)	(1:2:1)	2	(1:−1:−3:6)

The relevant quantities in Table 2 are substituted into Eq. (14), yielding three constraint hyperboloids in the image space. The points of intersection of all three quadrics (there can be at most six finite real ones) are the images of the forward kinematic solutions. Figure 4 shows the three quadrics projected on the hyperplane $X_4=1$. The three constraint equations are easily reduced to the following univariate in X_3:

$$4249X_3^6-1244X_3^5-1097X_3^4+200X_3^3-65X_3^2+4X_3+1=0. \tag{27}$$

This equation has six distinct roots, yielding the possible orientations of E relative to Σ (the orientation of the platform for the three given inputs):

$$X_3=-0.5120,-0.0858,0.1608,0.6345,0.0476+0.2241i,0.0476-0.2241i. \tag{28}$$

Back-substitution is used to determine the values of X_1 and X_2 corresponding to each real root of Eq. (27). The pre-image of each set of X_i is determined by repeated application of Eqs. (5). The four real poses of the platform resulting from the specific inputs are listed in Table 3. The resulting platform assembly modes are illustrated in Fig. 5, where each platform point is on the appropriate fixed centred circle.

6.2 Asymmetric *RPR*, *RPR*, *RPR* Platform. The general case of a three-legged platform can be demonstrated using a platform possessing three *RPR* legs where the active joint is different in each of the three legs: leg A is *RR*-type, leg B is *PR*-type, leg C is *RP*-type. This platform is also illustrated by Fig. 3. The relevant kinematic mapping parameters are listed in Table 4. The *fixed* base reference points $(X:Y:Z)$ are expressed by $F_{i/\Sigma}$. The *moving* platform points $(x:y:z)$ are expressed by $M_{i/\Sigma}$. The corresponding circle and line coefficients for the platform are determined by Eqs. (15), (20), and (22), respectively. The active *P*-pair input for leg A is specified by $r_A=2.5$. The active *R*-pair input for leg B is specified by the angle the passive *P*-pair makes with the X-axis, expressed in Σ. It is specified by $\beta_\Sigma=135°$. The active *R*-pair input for leg C is specified by the angle the passive *P*-pair makes with the x-axis, expressed in E. It is specified by $\gamma_E=45°$.

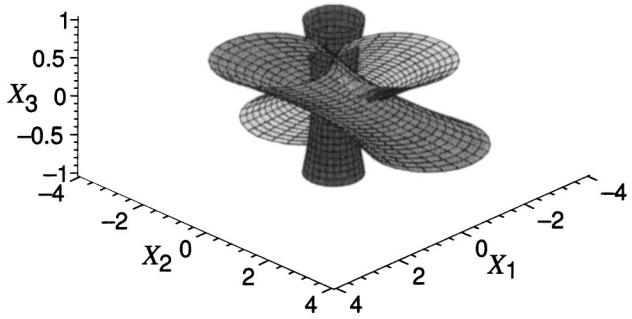

Fig. 4 The three constraint hyperboloids projected into the hyperplane $X_4=1$

Table 3 The four real *RPR* platform solutions

Solution	a	b	φ (deg.)
1	−0.0690	0.9976	−54.2255
2	−0.6290	−0.7773	−9.8079
3	−0.8916	−0.4529	18.2719
4	0.9829	−0.1841	64.7929

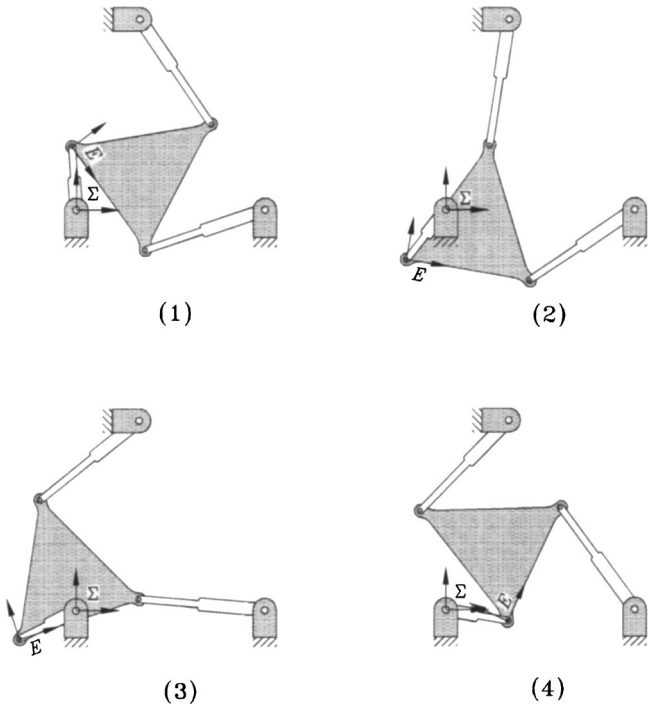

Fig. 5 The four real FK solutions for the symmetric *RPR* platform

The corresponding three constraint surfaces are an hyperboloid of one sheet for RPR leg A, an hyperbolic paraboloid for RPR leg B, and a kinematically inverted hyperbolic paraboloid for RPR leg C, see Fig. 6. The univariate in X_3 is computed together with corresponding real values of X_1 and X_2 for the real roots of the univariate, which in this case is 5th order:

$$45X_3^5-77X_3^4+56X_3^3+120X_3^2-53X_3+5. \tag{29}$$

The solutions must be carefully inspected. There are three real and one pair of complex conjugate roots. One root, $X_3=-1$, represents a line that is a common generator between the two hyperbolic paraboloids, but that does not intersect the hyperboloid in any finite points, see Fig. 6.

The two remaining real roots that lead to forward kinematic solutions are listed in Table 5. The kinematic mapping image of

Table 4 Kinematic mapping parameters of the asymmetric *RPR* platform

i	$F_{i/\Sigma}:(X:Y:Z)$	$M_{i/E}:(x:y:z)$	Input	$(K_0:K_1:K_2:K_3)$
A	(0:0:1)	(0:0:1)	$r=2.5$	(1:0:0:−25/4)
B	(6:0:1)	(2:0:1)	$\beta_\Sigma=135°$	$(0:-\sqrt{2}/4:-\sqrt{2}/4:3\sqrt{2})$
C	(3:6:1)	(1:2:1)	$\gamma_E=45°$	$(0:-\sqrt{2}/4:\sqrt{2}/4:-\sqrt{2}/2)$

Table 5 The two real Cartesian solutions for the asymmetric *RPR* platform

Solution	a	b	φ (deg)
1	2.2993	0.9814	29.0303
2	1.5837	1.9344	16.3404

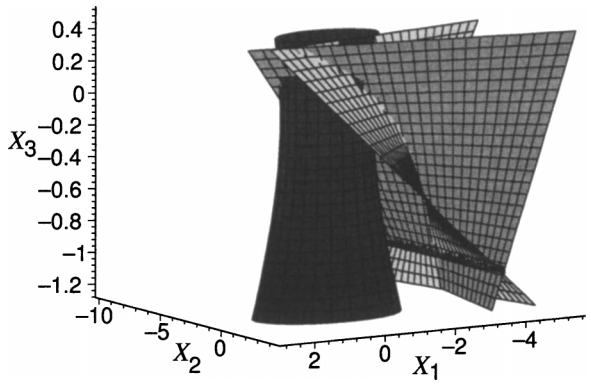

Fig. 6 The image of the two real FK solutions for the asymmetric *RPR* platform

the two solutions can be seen as the two points common to all three surfaces in Fig. 6, while the corresponding configurations are illustrated in Fig. 7.

6.3 Asymmetric Platform With One *PP*-Type Leg. The final example is included for completeness. Regardless of actuation topology, the *PP*-type leg input joint variable determines the platform orientation. Moreover, since no leg may be composed of three *P*-pairs, the third joint must be an *R*-pair. The platform in this example is composed of an $R\underline{P}R$ leg A, an $\underline{R}PR$ leg B, and an $\underline{R}PP$ leg C. As shown in Fig. 8, the knee-bend in leg C is 90°, which means that the platform orientation (the orientation of E with respect to Σ) is given explicitly by

$$\varphi = \gamma_\Sigma - 180°. \tag{30}$$

Thus, the image space coordinate $X_3 = \tan(\varphi/2)$, is defined by the input of leg C. The remaining image space coordinates are determined by the intersection of the plane defined by $X_3 = \tan(\varphi/2)$ with the other two constraint surfaces, which in this case are an hyperboloid and an hyperbolic paraboloid.

The platform geometry along with the three variable joint values which are listed in Table 6, yield the constraint surfaces shown in Fig. 9. Using these values, then setting $X_3 = \tan(10/2)$ after determining φ from Eq. (30), the following two equations are obtained, see Fig. 10:

$$X_1^2 + X_2^2 - 1.0077 = 0, \tag{31}$$

$$0.2281\sqrt{2}X1 - 0.2719\sqrt{2}X2 + 0.3380\sqrt{2} = 0. \tag{32}$$

The first, Eq. (31), is a circle and the second, Eq. (32), a line in the plane $X_3 = \tan(10/2)$ so as to yield the following:

$$X_1 = -0.8554, -0.3687$$

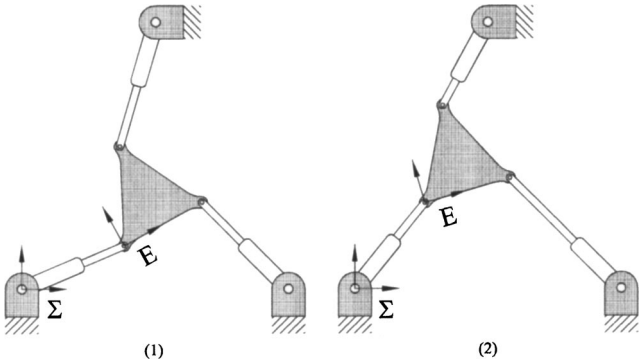

Fig. 7 The two real FK solutions for the asymmetric *RPR* platform

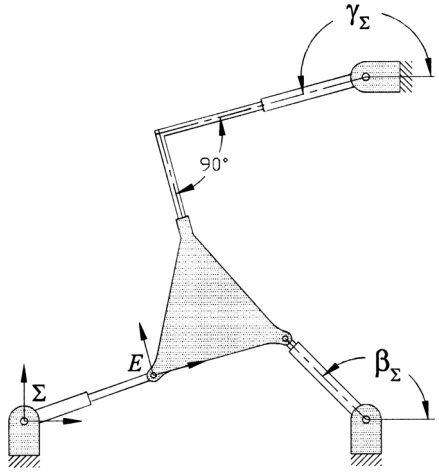

Fig. 8 *PP*-type leg *C*

$$X_2 = 0.5253, 0.9336$$

$$X_3 = 0.0875.$$

The form of these two curves of surface intersection, shown in Fig. 10, follows from the properties of the constraint surfaces [24]: hyperboloid sections in planes $X_3 = \text{constant}$ are always circles; one of the reguli of the hyperbolic paraboloid consists entirely of lines parallel to the planes $X_3 = \text{constant}$. Clearly, there are at most two solutions, which are listed in Table 7, and illustrated in Fig. 11. An interesting result to note is the symmetry in the Cartesian solution. While the symmetry seems reasonable *post hoc* (the joint angles β and γ along with the prismatic length r_A must be the same in both solutions), it is not *a priori* obvious. A forward kinematic computational advantage to such a platform is that only one solution branch needs to be determined.

7 Conclusions and Future Work

It was shown that there are 1653 distinct planar three DOF three-legged platform design layouts, jointed exclusively with lower pairs. The kinematics of all 1653 can be analyzed using the kinematic mapping based constraint formulation presented herein. For forward kinematic purposes the individual legs can be classified with only six distinct types of binary, passive joint combina-

Table 6 The asymmetric platform with one *PP*-type leg

Leg	Type	$F_{i/\Sigma}$	$M_{i/\Sigma}$	Input	$(K_0:K_1:K_2:K_3)$
A	$R\underline{P}R$	(0:0:1)	(0:0:1)	$r_A = 2$	(1:0:0:−4)
B	$\underline{R}PR$	(5:0:1)	(2:0:1)	$\beta_\Sigma = 135°$ (deg)	$(0:-\sqrt{2}/4:-\sqrt{2}/4:5\sqrt{2}/2)$
C	$\underline{R}PP$	(5:5:1)	(1:2:1)	$\gamma_\Sigma = 190°$ (deg)	$X_3 = \tan(10/2)$

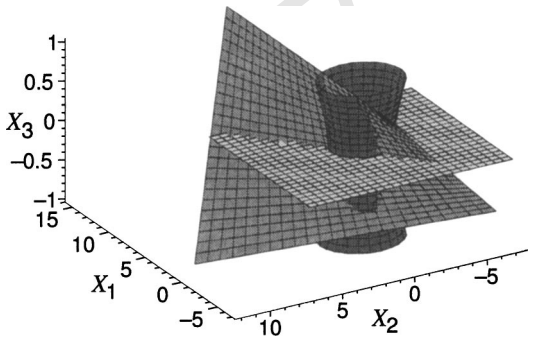

Fig. 9 The three constraint surfaces for the one *PP*-type leg platform

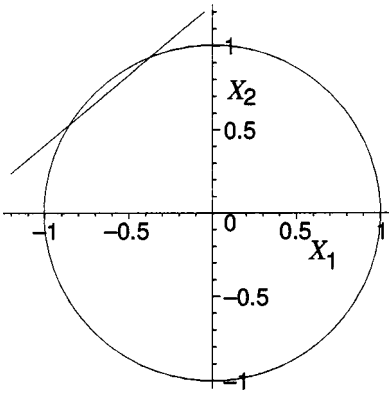

Fig. 10 Intersection of hyperbolic paraboloid and hyperboloid in the image plane of the *PP*-type leg

tion. The platform could be composed of three *RR*-type legs; any combination of three *PR*- or *RP*-type legs; two *RR*-type and one *PR*- or *RP*-type leg; one *RR*-type and any combination of two *PR*- or *RP*-type legs; two *RR*-type legs and one *PP*-type leg; one *RR*-type leg, one *PP*-type leg, and one *PR*- or *RP*-type leg. These are summarized in Table 8.

The forward kinematic problem reduces to determining the intersections among three constraint surfaces, one corresponding to each leg. For an *RR*-type leg the image space constraint surface is an hyperboloid of one sheet that contains circles in planes parallel to $X_3=0$. For both the *PR*- and *RP*-type legs the image space constraint surface is an hyperbolic paraboloid where one regulus contains lines parallel to $X_3=0$. Both of these quadrics are completely described by Eq. (14). The image space constraint surface for a *PP*-type leg is a plane parallel to $X_3=0$. The plane is determined by the tangent of one-half of the orientation angle of the platform, controlled by the active *R*-pair in the *PP*-type leg.

Table 7 The two real Cartesian solutions for the one *PP*-type leg platform

Solution	*a*	*b*	φ (deg)
1	1.7890	0.8940	10
2	0.8940	1.7890	10

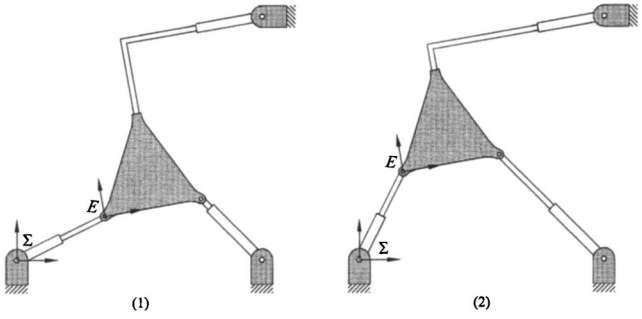

Fig. 11 The two real FK solutions for the one *PP*-type leg platform

Table 8 The six distinct types of planar three-legged platform with three DOF

Platform type	Leg combinations
I	3 *RR*
II	3 *PR* and/or *RP*
III	2 *RR* and 1 *PR* or *RP*
IV	1 *RR* and 2 *PR* or *RP*
V	2 *RR* and 1 *PP*
VI	1 *RR* and 1 *PP* and 1 *PR* or *RP*

The most important contribution of this work is that the forward kinematic problem of any planar three legged platform can be determined with a uniform procedure. Moreover, all solutions are always found. The solutions to inverse kinematic problems are found by solving individual constraint surface equations for the single unknown parameter given a platform pose which defines an image space point coordinate. This is done mostly so as to provide a readily understood relationship, in a simple context, between image space constructs and conventional Euclidean representation of kinematic concepts.

Future work includes derivation of an univariate with optimally reduced coefficients particularly applicable to real-time control of arbitrary planar three-legged platforms. Coefficients in the leg constraints will have to be preconditioned. Then an approach to back-substitution will be developed to ensure that each real solution to the univariate is deterministically matched with the corresponding pair of remaining image space coordinates in the forward kinematic solution. The kinematic constraint formulation will also be applied to develop unified workspace and singularity visualization schemes for such platforms.

References

[1] Blaschke, W., 1911, ''Euklidische Kinematik und Nichteuklidische Geometrie,'' Zeitschr. Math. Phys., **60**, pp. 61–91 and 203–204.
[2] Grünwald, J., 1911, ''Ein Abbildungsprinzip, welches die ebene Geometrie und Kinematik mit der räumlichen Geometrie verknüpft,'' Sitzber. Ak. Wiss. Wien, **120**, pp. 677–741.
[3] Study, E., 1903, *Geometrie der Dynamen.*, Teubner Verlag, Leipzig, Germany.
[4] Klein, F., 1872, ''Vergleichende Betrachtungen über neuere geometrische Forschungen, Erlangen,'' reprinted in 1893, Mathematische Annalen, **43**, pp. 63–100.
[5] Klein, F., 1939, *Elementary Mathematics From an Advanced Standpoint: Geometry*, Dover Publications, Inc., New York, N.Y.
[6] Rooney, J., and Earle, C. F., 1983, ''Manipulator Postures and Kinematics Assembly Configurations,'' *6th World Congress on Theory of Machines and Mechanisms*, New Delhi, pp. 1014–1020.
[7] Roth, B., 1993, ''Computations in Kinematics,'' *Computational Kinematics*, Angeles, J., Hommel, G., and Kovács, P., eds., Kluwer Academic Publishers, Dordrecht, The Netherlands, pp. 3–14.
[8] Roth, B., 1994, ''Computational Advances in Robot Kinematics,'' *Advances in Robot Kinematics and Computational Geometry*, Lenarčič, J., and Ravani, B., eds., Kluwer Academic Publishers, Dordrecht, The Netherlands, pp. 7–16.
[9] Shirkhodaie, A. H., and ane Soni, A. H., 1987, ''Forward and Inverse Synthesis for a Robot With Three Degrees of Freedom,'' *Summer Computation Simulation Conference*, Montréal, Qué, Canada, pp. 851–856.
[10] Gosselin, C., and Sefrioui, J., 1991, ''Polynomial Solutions for the Direct Kinematic Problem of Planar Three-Degree-of Freedom Parallel Manipulators,'' *Proc. 5th Int. Conf. on Adv. Rob. (ICAR)*, Pisa, Italy, pp. 1124–1129.
[11] Hunt, K. H., 1983, ''Structural Kinematics of In-Parallel-Actuated Robot Arms,'' ASME J. Mech. Des., **105**(4), pp. 705–712.
[12] Wohlhart, K., 1992, ''Direct Kinematic Solution of the General Planar Stewart Platform,'' *Proc. of the Int. Conf. on Computer Integrated Manufacturing*, Zakopane, Poland, pp. 403–411.
[13] Merlet, J.-P., 1996, ''Direct Kinematics of Planar Parallel Manipulators,'' *IEEE Int. Conf. on Robotics and Automation*, Minneapolis, pp. 3744–3749.
[14] Pennock, G. R., and Kassner, D. J., 1992, ''Kinematic Analysis of a Planar Eight-Bar Linkage: Application to a Platform-Type Robot,'' ASME J. Mech. Des., **114**(1), pp. 87–95.
[15] Pennock, G. R., and Kassner, D. J., 1993, ''The Workspace of a General Geometry Planar Three-Degree-of-Freedom Platform-Type Manipulator,'' ASME J. Mech. Des., **115**, pp. 269–276.
[16] Gosselin, C., 1988, ''Kinematic Analysis, Optimization and Programming of Parallel Robotic Manipulators,'' PhD thesis, Dept. of Mech. Eng., McGill University, Montréal, Qc., Canada.
[17] Murray, A. P., and Pierrot, F., 1998, ''N-Position Synthesis of Parallel Planar RPR Platforms,'' *Advances in Robot Kinematics: Analysis and Control*, Lenarčič, J., and Husty, M. L., eds., Kluwer Academic Publishers, Dordrecht, The Netherlands, pp. 69–78.
[18] Husty, M. L., 1995, ''Kinematic Mapping of Planar Tree(*sic.*)-Legged Platforms,'' *Proc. 15th Canadian Congress of Applied Mechanics (CANCAM 1995)*, Victoria, B. C., Canada, Vol. 2: pp. 876–877.
[19] Hayes, M. J. D., 1999, ''Kinematics of General Planar Stewart-Gough Platforms,'' PhD thesis, Dept. of Mech. Eng., McGill University, Montréal, Qc., Canada.
[20] Chen, C., 2001, ''A Direct Kinematic Computation Algorithm for all Planar 3-Legged Platforms,'' Master's thesis, Dep't. of Mech. Eng., McGill University, Montréal, Qc., Canada.

[21] Zsombor-Murrary, P. J., Chen, C., and Hayes, M. J. D., 2002, ''Direct Kinematic Mapping for General Planar Parallel Manipulators,'' *Proc. CSME Forum 2002*, Kingston, On., Canada.
[22] Hayes, M. J. D., Husty, M. L., and Zsombor-Murray, P. J., 1999, ''Solving the Forward Kinematics of a Planar 3-Legged Platform With Holonomic Higher Pairs,'' ASME J. Mech. Des., **121**(2), pp. 212–219.
[23] Bottema, O., and Roth, B., 1990, *Theoretical Kinematics*, Dover Publications, Inc., New York, N.Y.
[24] Hayes, M. J. D., and Husty, M. L., 2003, ''On the Kinematic Constraint Surfaces of General Three-Legged Planar Robot Platforms,'' Mech. Mach. Theory, **38**(5), pp. 379–394.
[25] Hayes, M. J. D., and Zsombor-Murray, P. J., 1996, ''A Planar Parallel Manipulator With Holonomic Higher Pairs: Inverse Kinematics,'' *Proc. CSME Forum 1996, Symposium on the Theory of Machines and Mechanisms*, Hamilton, On., Canada, pp. 109–116.
[26] Hayes, M. J. D., and Zsombor-Murray, P. J., 1998, ''Inverse Kinematics of a Planar Manipulator With Holonomic Higher Pairs,'' *Recent Advances in Robotic Kinematics*, Lenarčič, J., and Husty, M. L., eds., Kluwer Academic Publishers, Dordrecht, The Netherlands, pp. 59–68.

PROOF COPY 013405JMD